Answer to referee comments of referee 1

Dear Referee #RC1,

Thank you very much for your detailed feedback. It is very much appreciated and enhances our work!

Major comments

Excitation method: It is not very common to excite the blades in the blade coordinate system, simply because it is hard or even impossible to achieve in an experimental set-up. We have chosen this method, because we could achieve very clear spectra which is crucial for the damping estimation from peak-to-peak counting. Example spectra and a paragraph are. An example of the decaying time-series is also added together with the resulting estimated damping and the restrictions of the used method.

Analysis based on turbine with reduced flexibility: The reason to base the analysis on the RTT rotor is that with it is possible to capture the difference in edgewise whirl damping between the two rotor configurations (upwind and downwind) with the minimum degree of freedom. The fully flexible turbine has a lower damping especially for the forward whirl mode. However, these additional degrees of freedom have a similar impact on both, the upwind and the downwind configuration. Thus, these are not a causation of difference in edgewise loads that can be observed in load simulations.
The advantage of the reduced degrees of freedom is, that it allows to separate the motion of the substructure from the rotor motion without influence of interaction of the nacelle or shaft. This might on the other hand over pronounce the impact of the shaft length or the cone angle. However, it does show the trends and the difference in interaction of the rotor with the tower torsion which has been proven to have a big impact on the edgewise whirl damping. It should also be pointed out, that the absolute edgewise whirl damping is very turbine specific. Even with the full flexibility, this work shows the trends of change when changing the turbine configuration from upwind to downwind, and how the difference in damping can be influenced. Thus, the plots of the parameter variations cannot be compared to each other regarding absolute damping values.
A comment to this is added in the text for clarification.

Study of whirl characteristics with reduced degrees of freedom: As we have shown from the comparison of the fully flexible turbine configuration with the turbine configurations with reduced number of degrees of freedom, the difference in damping between the upwind and the downwind configuration can be captured. Including all degrees of freedom does change the whirl characteristics, especially through the tower flexibility. However, we could only observe small differences of the influence on the upwind configuration compared to the downwind configuration which is what this work focusses on.
Generally, this study should be extended in future work to get the full picture of the difference of whirl characteristics.
A comment to this is added in the discussion section.

Forward spelling: has been corrected.

Minor comments

Line 14-16: It is true, that also downwind turbines can be constraint in blade design depending on the geometrical configuration of the turbine as well as the design driving situations and the handling of fault situations by the controller. The introduction is changed accordingly.

Line 76-78: (The turbine flexibility is reduced to the rotor flexibility and tower torsional flexibility, as this configuration resembles the difference in edgewise damping with the minimum degrees of freedom.) The sentence is rephrased to: The resulting configuration consists of a fully flexible rotor and a tower that is only flexible in torsion. This configuration with reduced flexibility captures the main difference in edgewise whirl mode damping and allows a more detailed analysis of modal displacements.

Line 85: (coupling terms due to prebend and shaft tilt) The coupling terms are not expected to play a prominent role in the in-plane vibrations (This has been checked with hawcStab2 for the upwind configuration). They are neglected rather to avoid excitation of the out-of-plane modes from the forces that are used for excitation. Otherwise, the peak-to-peak counting used for damping estimation and especially the mode shape analysis are misleading. A comment on this has been added to the manuscript.

Line 96: (By setting gravity to zero, the variation of stiffness is neglected) It is assumed that the structural stiffness and the centrifugal effect are dominant and the variation of stiffness from gravity is negligible. However, this cannot be quantified by the chosen method as the rotation in the gravity field would permanently excite the in-plane blade motion which makes the damping prediction from the time-series impossible. HAWCStab2 as a tool is no alternative since it neglects the effect of gravity. Further analysis of this effect could be done with Floquet-analysis, but this is outside the scope of this work.

Section 2.2: (why only 9m/s?): 9m/s is chosen as the observed difference in damping so differences in modal displacements are expected to be largest.
(Distinguishing between self-motion and substructure motion): To be able to investigate the modal displacement the displacement of the blades is extracted in the blade coordinate system, while the displacement due to tower motion is extracted in the tower coordinate system. To be able to do the analysis of the contribution to out-of-plane motion all displacements need to be in the same coordinate system, which requires the Coleman-transformation. For the damping estimation, this would not be required. The text is adjusted for clarification.
(Procedure for phase consistency) This procedure is not standard practice. However, phase consistency has to be assured, as several spectra are calculated for each signal independently (blades and tower torsion). The implemented Matlab procedure gives a spectrum with relative phases for each spectrum. Further explanation is added.

Line 140: normalization definition is added.

Line 154-156: "Other degrees of freedom such as tower bending flexibility do influence the absolute damping of the whirl modes but do not cause the major differences between the upwind and the downwind configuration." Added as a comment in the text.

Line 155: The coinciding lines are not plotted and this is pointed out in the text as additional information.

Figure 2: The time-series are regenerated from the spectrum of the time-series to assure the displacement is a modal displacement. The damping is therefore not included. The information is added in the description of the method.

Line 203: Generic out-of-plane motion or due to the tower torsion? The "total" out-of plane motion is added to the text.

Line 206: the edgewise "whirl" damping is added to the text.

Section 3.2: The text is referring to the cosine component of the rotor contributing to 5% of the difference in the out-of-plane displacements (line 182-183) The substructure does not have a contribution to the cosine displacement since the tower bending is neglected.

Figure 3-5: "edgewise damping" has been replaced by "edgewise whirl damping"

Chapter 4 & Line 308-309: "Expected role of tower bending" expanded in section 5. The tower fore-aft bending is expected to be seen directly in the out-of-plane displacement. The tower side-side bending couples directly to the asymmetric edge whirl motion and can further be expected to couple to out-of-plane displacement through the yaw motion, as the center of gravity of the rotor nacelle assmbly is not at the tower center.

Line 204-205: total impact of low tower torsional stiffness on downwind configurations has not yet been investigated. For upwind configurations the lower edgewise damping for lattice structures is well known. Further investigations would need to be made and full load assessment would be required to fully evaluate the effect of the lower tower torsional stiffness.

Generally: Spelling and grammatical comments are implemented.

Answer to referee comments of referee 2

Dear Vasilis A. Riziotis,

Thank you very much for your detailed feedback. It is very much appreciated and improves our work!

__Main comments__

1.) Pros and Cons for damping assessment are added in the text. It is shown that there is only one frequency dominant in the time-series and examples are given. The generation of mode shapes is described in more details.
2.) A comparison of HAWC2 and HAWCStab2 for frequency and damping are added. Mode shapes could not be validated. The required mode shapes were not an official output from HAWCStab2 and needed post-processing from a binary file. It was possible to extract the amplitudes, but the phases could not be converted correctly for both edgewise whirl mode, even for the upwind configuration. The mode

shapes from HAWC2 on the other hand could be extracted in known coordinate systems and seemed to be consistent. However, there is no doubt that more work is required regarding a validation of the mode shapes.

3.) We checked that the DTU-10MW-RWT shows the same trend for the damping of the two edgewise whirl modes. However, how strongly this is pronounced is turbine specific. A comment is added in the discussion to point out to what extend the conclusions are turbine specific.

Supplement comments

Line 34: (Could you please become more specific. You are probably referring to bringing close to each other FW edgewise mode with the BW 2nd flap mode.) The 1st FW edge and 2nd BW flap mode have been added in the text.

Line 76-78: (The turbine flexibility is reduced to the rotor flexibility and tower torsional flexibility, as this configuration resembles the difference in edgewise damping with the minimum degrees of freedom.) The sentence is rephrased to: The resulting configuration consists of a fully flexible rotor and a tower that is only flexible in torsion. This configuration with reduced flexibility captures the main difference in edgewise whirl mode damping and allows more detailed analysis of modal displacements.

Line 97-98: (The controller is exchanged by a simple setting of pitch angle and rotational speed according to the wind speed at hub height to allow for a slow wind speed increase to avoid other modal frequencies than the excited frequencies in the timeseries.) Sentence is rephrased to: "[…] to avoid the excitation of modal frequencies other than the edgewise whirl frequencies. This resembles a fix-free drive train operational mode." The collective edgewise mode is not excited due to the chosen excitation method and the gravity set to zero. This has also been checked from the signal in the frequency domain. Otherwise, the estimation of damping from the time-series would be misleading.

Line 106-108: (It has been tested with the aeroelastic modal analysis tool HAWCStab2 (\cite{Hansen2004}) that the trends over wind speed as well as trends for the difference of damping between the configurations are captured correctly for investigations of qualitative differences. "This was done for the validation of the nonlinear damping characterization method and I suppose it was performed for the upwind turbine. Is that correct?") This has been done for validation of the nonlinear damping characterization method of both upwind and downwind configuration. HAWCStab2 agrees with the change of damping over wind speed, as well as, the ratio of damping between the upwind and the downwind configuration. However, the absolute values are not the same and more investigations are needed.
We have also tried to validate the mode shapes between HAWC2 and HAWCStab2, but the phases do not agree. We assume, that this is an issue of the output file generated by HAWCStab2, as the sorting of mode shapes and coordinate-systems of the auto-generated data could not be clarified, especially for the downwind configuration.

Line 109-111: (For a primary damping estimation the damping coefficient for a single airfoil as described by Hansen (2007) is calculated.) Text is changed for clarification of the aim, namely to assure that differences of damping are not due to operational points of the airfoil and/or the steady states of the turbine configurations.

Line 127-132: (Calculation of modal displacement and phase consistency). The section has been extended as it caused confusion. No direct system identification method has been used. It has been assured, that the method of excitation only excites one of the whirl modes, which has been checked from the spectra. Mode shapes are then calculated from the frequency and phase information of the spectra. An additional explanation has been added. The method of phase consistency has been described in more detail as there is no reference and it might not be a common standard.

Line 134: Validation for the frequency and damping has been added. The mode shapes could not be validated, due to unresolved issues with the output from HAWCStab2. (The output does not agree with the internal animation inside HAWCStab2.) The latter is the main reason to finally do the study with HAWC2.

Line 140: normalization definition is added.

Line 289: A paragraph is added to explain to what extend the conclusions and results are turbine specific.

Generally: Spelling and grammatical comments are implemented.

Differences in damping of edgewise whirl modes operating an upwind turbine in a downwind configuration

Gesine Wanke[1], Leonardo Bergami[1], and David Robert Verelst[2]

[1]Suzlon Blade Science Center, Havneparken 1, 7100 Vejle, Denmark
[2]DTU Wind Energy, Technical University of Denmark, Frederiksborgvej 399, 4000 Roskilde, Denmark

Correspondence: Gesine Wanke (gesine.wanke@suzlon.com)

Abstract. The qualitative changes in damping of the first edgewise modes when an upwind wind turbine is converted into the respective downwind configuration are investigated. A model of a Suzlon S111 2.1MW turbine is used to show that the interaction of tower torsion and the rotor modes is the main reason for the change in edgewise damping. For the forward whirl mode, a maximum decrease in edgewise damping of 39% is observed and for the backward whirl mode, a maximum increase of 18% in edgewise damping is observed when the upwind configuration is changed into the downwind configuration. The shaft length is shown to be influencing the interaction between tower torsion and rotor modes as out-of-plane displacements can be increased or decreased with increasing shaft length due to the phase difference between rotor and tower motion. Modifying the tower torsional stiffness is seen to give the opportunity in the downwind configuration to account for both, a favorable placements of the edgewise frequency relative to the second yaw frequency, as well as a favorable phasing in the mode shapes.

1 Introduction

Upwind wind turbines, where the rotor is placed in front of the tower relative to the wind, have been in the focus of research efforts for the recent years. As wind turbines increase in size ~~, and~~ and the cost of energy has to be reduced, rotor blades become longer and increase in flexibility. The blade tip to tower clearance is a constraint for the design of such blades. ~~Downwind~~ For downwind rotors, where the rotor is placed behind the tower ~~are not subject to such constraint~~ this constraint is relaxed during normal operation and downwind rotors re-experience therefore an increase in the research effort.

The downwind concepts are known to show a higher fatigue load for the flapwise blade root moments compared to the upwind concepts due to the tower shadow effect. Glasgow et al. (1981) measured a significant fatigue load increase in the flapwise bending loads for a downwind configuration compared to an upwind configuration of a 100kW machine due to the velocity deficit of a truss tower. Zahle et al. (2009) ~~simulated~~ predicted a reduction in normal force on the blade of 20%, due to the rapid fluctuation in the angle of attack as the blade passes through the tower wake. A fatigue load increase of around 20% for the damage equivalent flapwise blade root bending moment was found by Reiso and Muskulus (2013) ~~,~~ when comparing the

5MW NREL reference turbine in a downwind configuration to the original upwind configuration.

A comparison of a full design load basis for a commercial Suzlon class IIIA 2.1MW wind turbine in an upwind configuration and a downwind configuration by Wanke et al. (2019) showed, that also the edgewise fatigue load increases significantly when changing the upwind configuration into a downwind configuration. Only 30% of the fatigue load increase for the edgewise blade root sensor could be associated with the tower shadow effect. The remaining fatigue load increase could be associated with a lower edgewise damping in the forward whirl mode of the downwind configuration.

In the 1990s first research efforts were made to characterize the damping of the edgewise blade modes since some stall regulated turbines showed stall induced vibrations. Petersen et al. (1998a) described how the local edgewise vibrations coupled to the substructure in global forward (FW) and backward (BW) whirling modes. The whirling modes resulted in a force at the hub center, rotating either with the rotational direction of the shaft (FW) or against the rotational direction of the shaft (BW). Energy was seen to be exchanged between the blade and rotor modes if the frequencies of the first edgewise FW mode and the second flapwise BW mode were placed close together. Lower damping of the modes was shown to lead to a significant increase in both fatigue and extreme loads as vibration amplitudes are higher.

In the 'STALLVIB'-project Petersen et al. (1998b) aimed to predict margins of damping, identify important parameters influencing the edgewise damping and to establish design guidelines to prevent the occurrence of stall induced vibrations. It was seen that the aerodynamic damping determined if stall induced vibrations would occur. The out-of-plane motion could generally be associated with higher aerodynamic damping. Airfoil characteristics such as the stall behavior and the slope of the lift curve over the angle of attack were found to determine if the aerodynamic force created from the vibration velocity restored the steady-state position.

Thomsen et al. (2000) used a rotating mass on the nacelle to excite the edgewise whirling modes of a 600kW upwind turbine. From the measured blade root moment, the damping for the edgewise whirling modes was calculated. The results showed that the edgewise forward whirling mode was significantly higher damped than the corresponding backward whirling mode.

Hansen (2003) build a linearized model with 15 degrees of freedom to determine the damping for the edgewise modes of the turbine, measured by Thomsen et al. (2000), using an eigenvalue approach. Hansen could confirm that the edgewise forward whirl mode was significantly higher damped than the edgewise backward whirl mode. From the visualization of the modal amplitudes, it could be shown that the edgewise forward whirl mode had a significantly higher out-of-plane component than the backward whirl mode, contributing positively to the damping. The work recommended that the overall edgewise damping could be significantly increased if the turbine design was able to place the edgewise blade frequency between the 2nd yaw and tilt frequency of the turbine, as this increased the out-of-plane contribution of the edgewise forward whirl mode.

In the description of aeroelastic instabilities Hansen (2007) derived the aerodynamic damping coefficient of a single airfoil in dependency on the vibration direction. From the simplified analysis, he was able to show how the aerodynamic damping relates to the inflow velocity, the airfoil coefficients and the airfoil coefficient slopes over the angle of attack for different quadrants of vibration direction.

This paper focuses on the difference in edgewise damping when the Suzlon S111 2.1MW wind turbine is changed from an upwind configuration into a downwind configuration. The damping of the edgewise whirl modes will be estimated from time-series of the two turbine configurations and different sets of flexibility in the components. Finally, shaft length, cone angle and tower torsion are varied to show how the edgewise damping could be influenced by the turbine design.

The interaction of the rotor and the tower torsion will be shown to cause differences in the maximum damping between the two edgewise whirl modes and the two turbine configurations. The interaction of the edgewise forward whirl mode and the tower torsion increases the edgewise damping in the upwind configuration and decreases the edgewise damping in the downwind configuration. In the forward whirl mode the edgewise damping decreases by 39% when the S111 Suzlon turbine is changed from the upwind configuration into a downwind turbine. In the backward whirl mode, the damping increases 18% when the S111 Suzlon turbine is changed from an upwind configuration into a downwind configuration. Differences in out-of-plane displacements cause the main difference in damping between the two turbine configurations and the two modes. As the eigenfrequency of the edgewise forward whirl mode is closer to the second yaw frequency the forward whirl mode will show a higher difference in damping between the configurations. The difference in damping of the forward whirl mode dominates, therefore, the overall change in damping when the upwind configuration is changed into the downwind configuration, as well as the difference in extreme and fatigue loads.

2 Methods

In this study, two different attempts are made to investigate the difference in edgewise damping between an upwind configuration and a downwind configuration. Firstly, the edgewise damping of the full turbine is calculated from HAWC2 (Madsen et al. (2020) (Version 12.7)) time-series for upwind and downwind configuration with the full turbine flexibility, called the fully flexible (FF) configurations. Further, the edgewise damping is estimated for turbine configurations with reduced flexibility. The flexibility is reduced by increasing the stiffness of certain turbine components significantly. The resulting configuration consists of a fully flexible rotor and a tower that is only flexible in torsion. This configuration with reduced flexibility captures the main difference in edgewise whirl mode damping between the upwind and the downwind configuration and allows more detailed analysis of modal displacements (see also Fig. 4). The configurations with reduced flexibility are called the upwind RTT (rotor and tower torsion) and the downwind RTT configuration.

Secondly, the influence of shaft length, cone angle and tower torsional stiffness on the edgewise damping of the upwind RTT and downwind RTT configuration are studied by parametric variation. The influence of the shaft length is investigated in a range of -30% and +100%, the cone angle, coning away from the tower from 0° to 7.5° and the tower torsional stiffness in a range of ± 80%. Table 1 shows a summary of all the configurations used in the study and the investigated parameter variation. The study is based on a Suzlon S111 2.1MW, class IIIA turbine with a rotor diameter of 112m and a 90m tubular

Table 1. Configurations and parameter variations

configuration/ parameter variation	properties
edgewise damping estimation	
all configurations	no tilt, no cone, no prebend
	simplified controller, no gravity, uniform inflow
	(no turbulence, no sheer, no veer, no inclination angle)
upwind FF	upwind, all degrees of freedom (fully flexible)
downwind FF	downwind, all degrees of freedom (fully flexible)
upwind RTT	upwind, rotor flexibility, tower torsion flexibility
downwind RTT	downwind, rotor flexibility, tower torsion flexibility
parameter variation	
shaft length	up- and downwind RTT configuration
	shaft length variation: -30% to +100%
cone angle	up- and downwind RTT configuration
	cone angle variation: 0° to 7.5° (away from tower)
tower torsional stiffness	up- and downwind RTT configuration
	torsional stiffness factor variation $\pm$ 80%

~~tower height~~height tubular tower. The turbine is pitch regulated and operating at variable rotor speed below rated power. The operational range is from $4\mathrm{ms}^{-1}$ to $21\mathrm{ms}^{-1}$ and rated wind speed is $9.5\mathrm{ms}^{-1}$. Blade prebend and shaft tilt are neglected in the study to reduce coupling terms between in-plane and ~~out-of plane modes.~~ out-of-plane modes. This assures that exclusively the edgewise whirl mode is excited with the chosen method of excitation. The cone angle is neglected other than for the parameter
95 study for the same reason. The turbine is assembled as a downwind configuration by shifting the rotor behind the tower and yawing the shaft by 180°.

2.1 Damping estimation from ~~timeseries~~time-series

The damping of the turbine edgewise whirl modes is estimated from HAWC2 ~~(Madsen et al. (2020) (Version 12.7))~~ ~~timeseries~~time-series.
100 Alternatively, HAWCStab2 (Hansen (2004)) could be used to solve a linearised stability model around the non-linear deflected steady state. In doing so, the eigenfrequencies, damping and ~~modeshapes~~ mode shapes can be obtained directly by solving an eigenvalue problem of the linearised system. However, due to unresolved issues with respect to ~~modelling downwind turbines in~~ the reconstruction of mode shapes from the available HAWCStab2 ~~(which has only been used and tested in the traditional~~

4

upwind context) it was considered outside the scope of this investigation to address those challenges. output, HAWC2 was chosen for the present study.

The turbine configurations from Tab. 1 are subject to a uniform wind field without turbulence, wind shear or tower shadow, to reduce the noise in the ~~timeseries~~ time-series. The gravity is set to zero to avoid excitation with the rotational frequency on the edgewise signal. The controller is exchanged by a simple setting of pitch angle and rotational speed according to the wind speed at hub height to allow for a slow wind speed increase to avoid ~~other modal frequencies than the excited frequencies in the timeseries.~~ the excitation of modal frequencies other than the edgewise whirl frequencies. This resembles a fix-free drive train operational mode. A long run-in time is used to assure that the ~~steady state~~ steady-state positions of the turbine are reached and the noise from the run-in does not disturb the vibration signal. ~~The forward~~

The forward and backward edgewise whirl ~~mode~~ modes are excited with a harmonic force at the blade at around r/R=75% radius with the blade edgewise frequency in the blade coordinate system. A time shift of 1/3 of the vibration period between the excitation forces on the three blades assures that either the forward whirl mode or the backward whirl mode ~~are~~ is excited. The ~~foreward~~ forward whirl mode is ~~exited~~ excited with the blade order 3-2-1, as the blades are named in the tower passing order seen from the front. The backward whirl mode is excited with the blade excitation order 1-2-3. After the excitation has stopped, 10 seconds of the ~~timeseries~~ time-series signal are neglected and 50 seconds are used for estimation of damping of the edgewise modes. ~~It has been tested with the aeroelastic modal analysis tool HAWCStab2 (Hansen (2004)) that the trends over wind speed as well as trends for the difference of damping between the configurations are captured correctly for investigations of qualitative differences.~~

~~For a primary damping estimation~~ The excitation method of harmonic forcing with phase shift within the blade coordinate system would be rather difficult, if not impossible in an experimental set-up. However, it gives the opportunity in a simulation framework to excite the whirl modes separately. Figure 1 shows the spectra of the ~~damping coefficient for a single airfoil as described by Hansen (2007) is calculated. The damping coefficient is calculated from simulated steady state values of the airfoil coefficients and angle of attack at 9m/s, -3° pitch angle and r/R=75% rotor radius~~ in-plane displacements for the fully flexible turbine configurations in Coleman-coordinates, obtained with the described excitation method. The figure shows that the excitation method achieves a spectrum where the symmetric component is negligible, as the amplitude significantly smaller than the amplitude of the asymmetric whirl modes. Further, Fig. 1 shows that a dominating backward ((a) and (c)) or forward whirl mode ((b) and (d)) is achieved. It is crucial for the chosen method of damping estimation that exceptionally only one of the whirl modes is excited. It has been checked that this is the case for all the regarded time-series.

~~From the timeseries~~ From the time-series, the logarithmic damping decrement of the edgewise modes is extracted. For the estimation of damping the decaying displacement signal of the 3 blades at r/R=75% radius is used. The logarithmic damping decrement δ is calculated via

$$\delta = \frac{1}{N} ln \frac{x(t)}{x(t+NT)} \tag{1}$$

where N is the number of positive successive peaks, $x(t)$ is the edgewise displacement amplitude of the first peak and $x(t+NT)$ is the amplitude of the Nth peak at N vibration periods T after the first peak. The logarithmic damping decrement
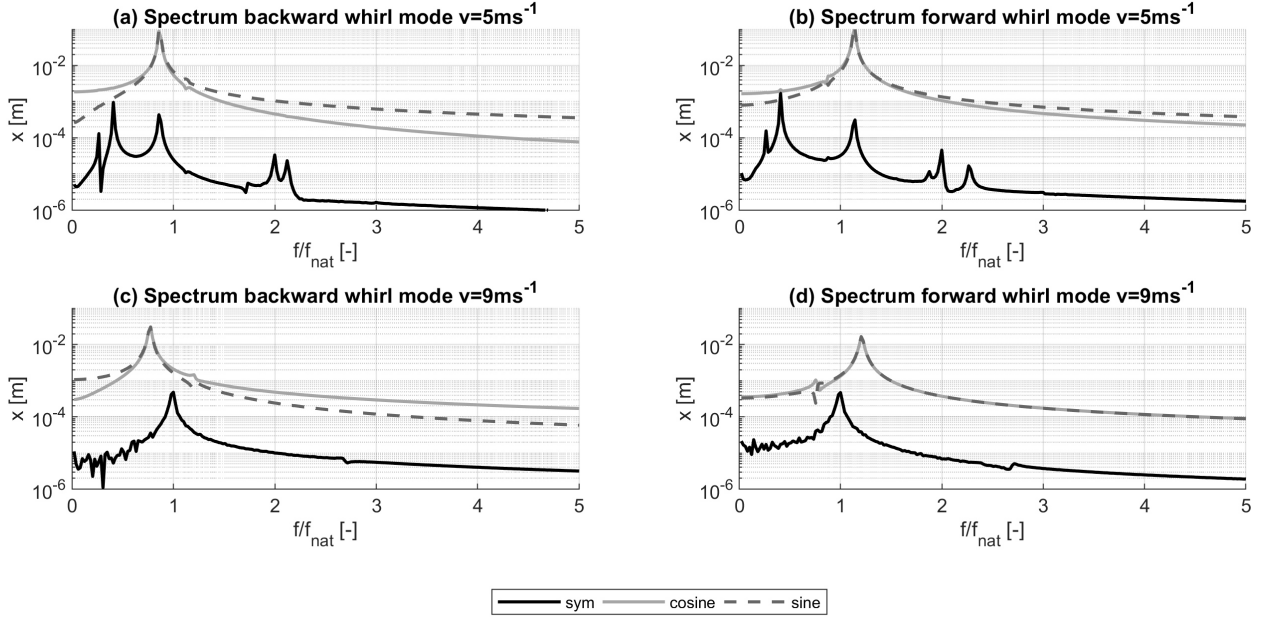
Figure 1. Spectrum of the in-plane displacements from time-series at 9ms^{-1} for the fully flexible turbine configurations in Coleman-coordinates for the backward whirl mode of the upwind configuration (a), the forward whirl mode of the upwind configuration (b) and the backward and forward whirl mode of the downwind configuration ((c) and (d)). The frequency axis is normalized with the blade edgewise natural frequency.

is converted to the damping ratio ζ

$$\zeta = \frac{1}{\sqrt{1 + \left(\frac{2\pi}{\delta}\right)^2}} \tag{2}$$

140 The damping ratio is estimated from simulations for the backward and ~~foreward~~ forward whirling mode of the fully flexible (FF) configurations as well as the upwind RTT and the downwind RTT configuration over the range of operational wind speeds. Figure 2 shows four time-series for the upwind FF configuration for the two whirl modes at 5ms^{-1} and 9ms^{-1} wind speed, as well as the decay function with the estimated logarithmic damping decrement. It can be seen, that generally a good estimate of damping is possible, especially if the damping is low, as shown in the time-series of 5ms^{-1}. As the damping increases the

145 method becomes less accurate as the detection of the peaks becomes more difficult as seen from in the time-series of 9ms^{-1}. As this method is using the same model as used for load simulations the method has the advantage of estimating directly the differences in damping without linearization effects. However, this method will only be able to estimate the damping, if clearly only one mode is excited and only one frequency dominates the spectrum (see also Fig. 1). The damping has to be so low that the peak to peak counting and amplitude detection can be reliably performed. This limited effectively the investigated range

150 of the investigated parameter. The edgewise modes are well suited for this method as they are significantly lower damped than
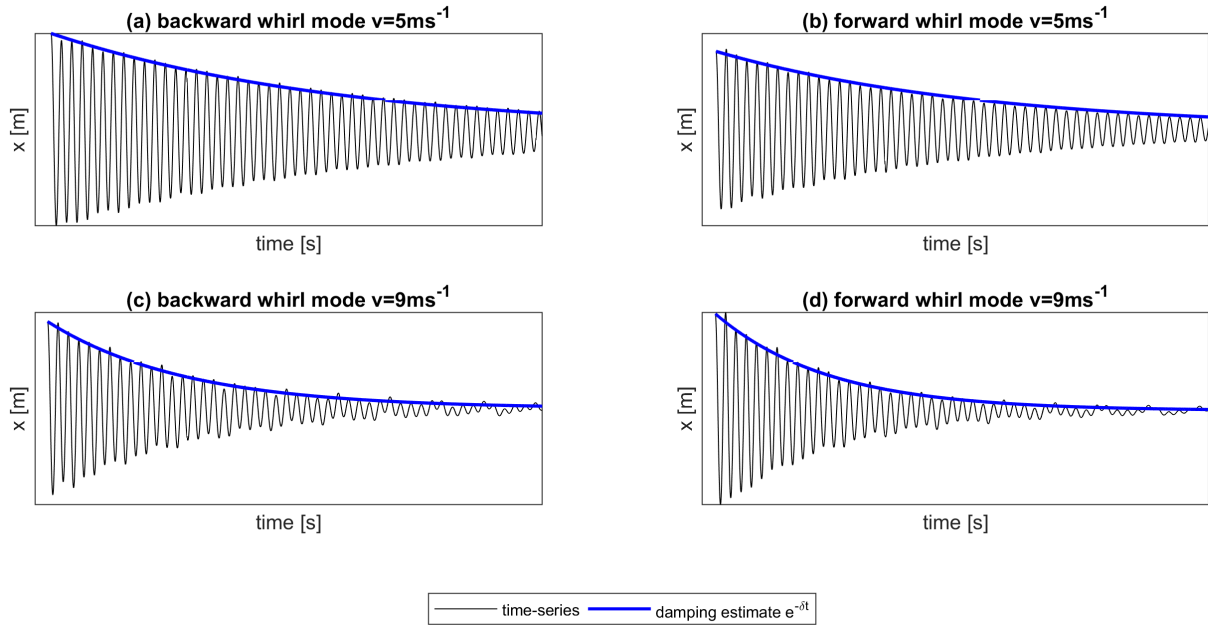
Figure 2. Example of estimated damping for an edgewise displacement time-series of the fully flexible upwind configuration at the backward whirl mode ((a) and (c)) and the forward whirl mode ((b) and (d)) for simulations of 5ms^{-1} and 9ms^{-1} wind speed.

other modes. Estimating the damping from an eigenvalue solution instead would eliminate these limitations.

The aeroelastic modal analysis tool HAWCStab2 (Hansen (2004), (Version 2.15)) has been used to calculate the eigenfrequencies of the edgewise whirl mode for the excitation. HAWCStab2 has further been used to validate the trend of the damping over wind speed for both turbine configurations, as well as the ratio of damping between the upwind and the downwind configuration.

155 The upper method is therefore assumed to be suitable for the investigation in this study.

According to Hansen (2007) the aerodynamic damping can be estimated for a single airfoil. This primary damping estimation is used to identify potential reasons for the difference in damping due to the steady-state and operational point of the airfoils of the upwind and the downwind configuration, as well as the in-plane velocity of the airfoil. The damping coefficient is calculated from simulated steady-state values of the airfoil coefficients and angle of attack at 9m/s, -3° pitch angle and r/R=75% rotor

160 radius, as well as the respective airfoil velocity.

2.2 Coleman transformed ~~timeseries~~time-series

By transforming the velocities and displacements to multiblade- or ~~coleman-coordinates~~ Coleman-coordinates (Bir (2008)) the difference in damping for the ~~timeseries~~ time-series at 9ms^{-1} can be further investigated. The time-series at 9ms^{-1} were chosen

7

165 as the difference in damping between the two turbine configurations was observed to be largest. For the r/R=75% airfoil section of the upwind RTT and downwind RTT configuration the velocities and displacements are transformed to ~~coleman-coordinates~~ Coleman-coordinates such that the components due to the blade self-motion as well as the motion of the substructure can be considered. The ~~later~~ latter is the motion of the non-deflected blade due to the tower torsion. To be able to distinguish the two components of the motion the tower torsion is monitored in the tower coordinate system, while the blade motion is monitored in

170 the blade frame of reference. Thus, the Coleman-transformation is required to monitor all signals in the non-rotating reference frame.

A Fourier-transformation is used to calculate the spectrum of the time-series. As clearly only one mode is excited, the modal displacements and velocities can be extracted from the spectrum. The modal displacement and modal velocities of the r/R=75% rotor position in the ~~coleman coordinates~~ Coleman-coordinates have been calculated via ~~fft-analysis in Matlab . In order to keep~~

175 ~~a global reference phase for all signals between the different fft-calculations the fft-analysis is once done on the original signal and once on the signal where the azimuth~~ a discrete Fourier transformation (FFT) in Matlab (MathWorks (2020)) for the component of the rotor self-motion as well as the motion of the substructure. The FFT-analysis returns the amplitude as well as the phase of the displacements. As the phase signal is relative information for each spectrum, the following procedure is chosen to assure the phase consistency between several FFT-analysis:

180 For each displacement signal (the three Coleman-coordinate signals and the tower torsion signal) the FFT-analysis is performed, resulting in the original spectrum. In a second step, the signal of the rotational position with a factor of 1/1000 is added ~~. From the comparison of the~~ to the displacement signal and a second spectrum is calculated (modified spectrum). From both spectra, the phase of the edgewise whirl mode frequency is extracted. The phase signal of the modified spectrum is shifted by the difference between the two edgewise signals such that the two signals have the same phase on the edgewise whirl frequency.

185 $$\phi_{modified,shifted} = \phi_{modified} - \phi_{modified,mode} + \phi_{original,mode} \tag{3}$$

where $\phi_{modified,shifted}$ is the resulting shifted phase of the modified spectrum, $\phi_{modified}$ is the phase information of the modified spectrum, $\phi_{modified,mode}$ and ϕ_{mode} are the phase of the edgewise whirl mode frequency for the modified and original signal. From the shifted, modified signal the phase information at the rotational frequency is extracted. The phase information of the original signal $\phi_{original}$ is then shifted by the phase of the rotational frequency of the shifted and modified

190 signal $\phi_{modified,shifted,rotation}$, such

$$\phi_{original,shifted} = \phi_{original} - \phi_{modified,shifted,rotation} \tag{4}$$

The shifted original signal $\phi_{original,shifted}$ aligns the phases such that the phase of the ~~original signal and the phase of the signal including the azimuth position all signals can be referenced to the phase of the global azimuth position. This guaranties~~ rotational signal is 0. This procedure guarantees, that the phasing between the substructure motion and the rotor

195 ~~modes~~ motion are consistent between several ~~fft-calculations.~~ FFT-calculations.

From the original, phase-shifted spectra the amplitude and phase information at the modal frequency of edgewise whirl modes is used to reconstruct the time-series of the modal displacement of the rotor as well as the modal displacement of the substructure.

This is equivalent to the inverse Fourier-transformation for a single frequency of the spectrum, namely the regarded whirl frequency. The modal velocities are calculated as the derivative of the modal displacements.

3 Results

The result section presents the ~~estimated~~ validation of the frequencies and estimated damping from HAWC2 against HAWCStab2. The section further shows the estimated edgewise damping as a function of wind speed for the fully flexible up-and downwind FF configuration as well as the up-and downwind RTT configuration. ~~Further the~~ The out-of-plane displacement of the edgewise modes is shown to be the reason for the difference in damping. Finally, the damping for the parameter variation for shaft length, cone angle, and tower torsional stiffness is presented.

3.1 ~~Edgewise~~ Validation of whirl frequencies and damping ~~over wind speed estimated from timeseries~~ between HAWC2 and HAWCStab2

Figure 3 shows the validation of the frequencies and the damping from the estimation in HAWC2 against the calculations with HAWCStab2 for the fully flexible turbine configurations as well as the two edgewise whirl modes. The figure shows that the frequencies calculated by HAWCStab2 and the frequencies extracted from the spectrum of HAWC2 time-series agree well. Small differences can be observed due to the resolution of the frequency axis of the spectrum. In Fig.3 (c) and (d) it can be seen that the general change in damping over wind speed is captured by the damping estimate. Also, the changes in damping when converting an upwind configuration into a downwind configuration are captured. However, the absolute damping values estimated from the HAWC2 time-series and calculated by HAWCStab do not agree over the full wind speed range for neither configuration or whirl mode. The HAWC2 estimations predict a higher damping in the backward whirl mode around rated power than the HAWCStab2 calculations. In the forward whirl mode, the HAWC2 estimations predict higher damping for high wind speeds than the HAWCStab2 calculations. Figure 1 ((a) and (b)) showed that the HAWC2 time-series were clearly dominated by the edgewise whirl frequencies for the fully flexible upwind configuration. Figure 2 ((c) and (d)), further showed that for the upwind configuration $9 \, \mathrm{ms}^{-1}$ the damping of both modes should be equally well estimated from HAWC2 time-series. Thus, the difference in estimated damping between HAWC2 and HAWCStab2 for the fully flexible upwind configuration at $9 \, \mathrm{ms}^{-1}$ observed in the backward whirl mode is not due to the method of damping estimation used for the HAWC2 time-series. It should be mentioned that HAWC2 and HAWCStab2 have slightly different implemented damping models which should explain the observed differences. As the differences in damping between the turbine configurations are captured correctly, the method of damping estimation from HAWC2 is assumed to be suitable for further investigations of damping difference in the edgewise whirl modes between the upwind and the downwind configuration.

3.2 Edgewise damping over wind speed estimated from time-series

Figure 4 shows the estimated normalized damping ratio as a function of wind speed for the backward (Fig. 4 (a)) and ~~foreward~~ forward whirl mode (Fig. 4 (b)) for the fully flexible up- and downwind FF configuration, as well as the upwind RTT and
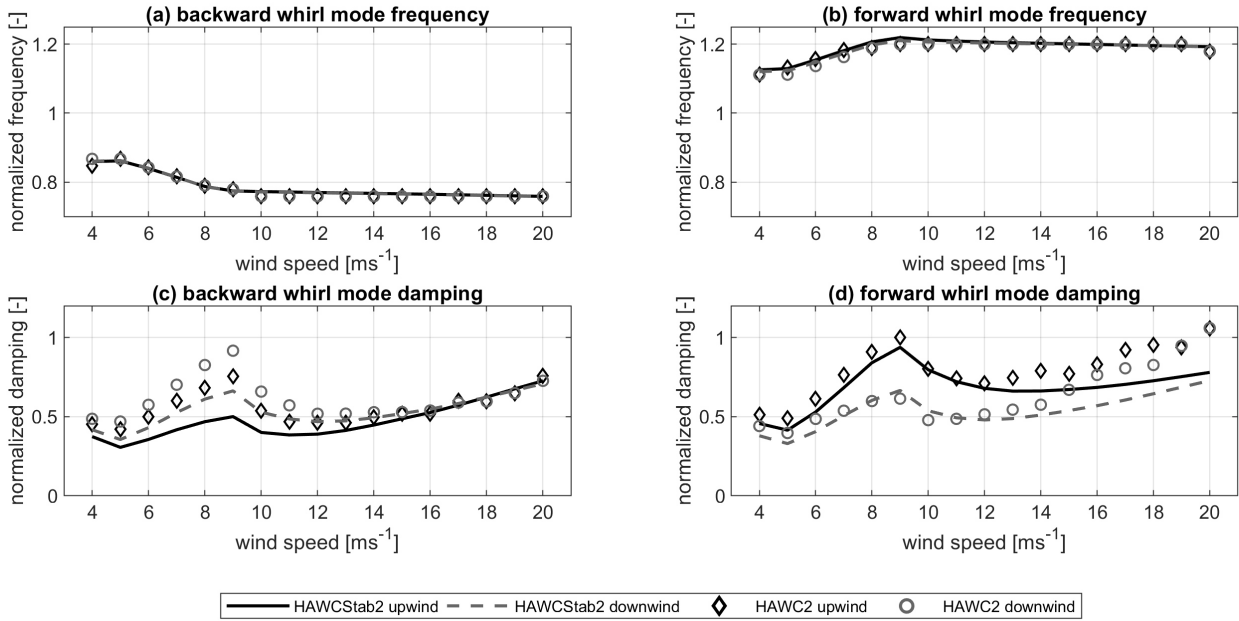
Figure 3. Normalized edgewise frequencies for the back whirl mode (a) and the forward whirl mode (b) for the upwind FF and the downwind FF configuration, as well as the damping of the backward whirl mode (c) and the forward whirl mode (d). The frequencies are normalized with the blade natural edgewise frequency, the damping is normalized with the damping of the upwind FF configuration at 9 ms^{-1} of the forward whirl mode from the HAWC2 estimation.

downwind RTT configuration. The figure further shows the difference in damping between the upwind configuration RTT and

230 the other configurations (Fig. 4 (c) and (d)).

Both, the damping as well as the damping difference are normalized with the damping of the upwind RTT configuration at 9 ms^{-1} of the forward whirl mode. The figure shows that both edgewise whirl modes in both configurations are positively damped. The damping ratio increases from cut-in wind speed to a local maximum at rated wind speed. After decreasing for wind speeds between rated wind speed and wind speeds around 14ms^{-1}, a damping increase for wind speeds higher than

235 14ms^{-1} is observed. In the backward whirl mode (Fig. 4 (a)) the downwind configurations are subject to higher edgewise damping than the respective upwind configurations. The difference is approximately 18% for the RTT configurations (see Fig. 4 (c)). In the ~~foreward~~ forward whirling mode (Fig. 4 (b)) the two downwind configurations are subject to significantly lower edgewise damping than the respective upwind configurations over the investigated wind speed range. The difference in edgewise damping is largest around rated wind speed, where the damping is approximately 39% lower in the downwind RTT

240 configuration than the upwind RTT configuration (Fig. 4 (d)).

For the upwind configurations the ~~foreward~~ forward whirl mode (Fig. 4 (b)) is significantly higher damped than the backward whirl mode (Fig. 4 (a)), as also shown by Hansen (2003), since the ~~foreward~~ forward whirl mode has a higher out-of-plane
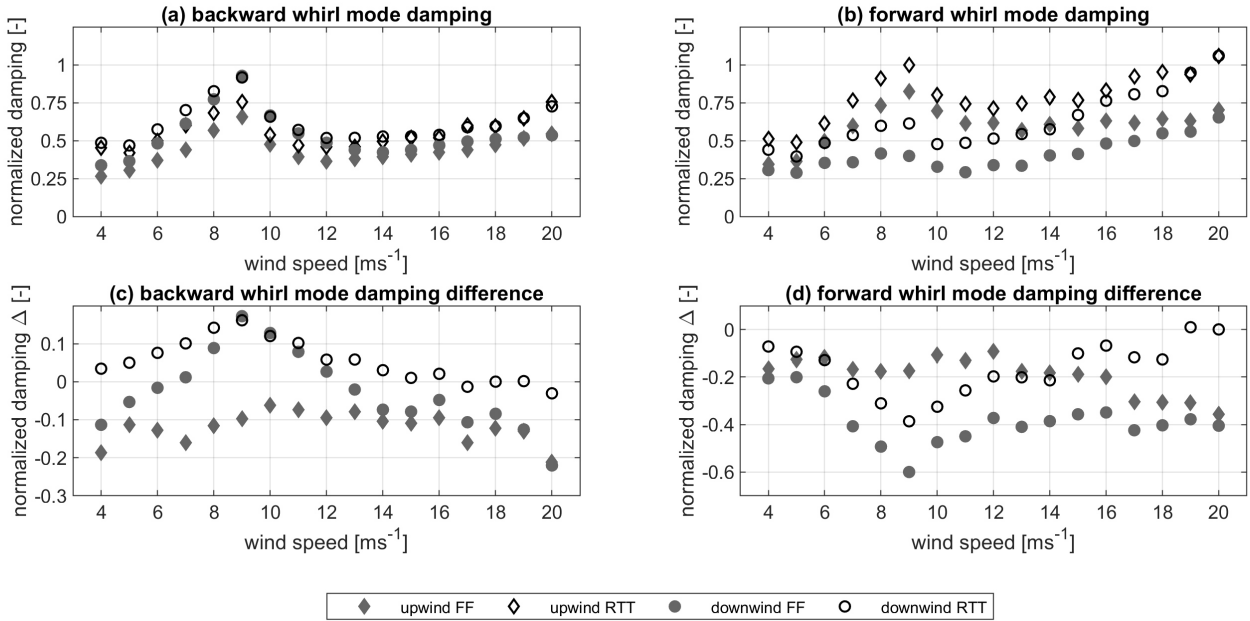
10

Figure 4. Normalized damping ratio as function of wind speed for the ~~back~~ edgewise backward whirl mode (a) and the ~~foreward~~ forward whirl mode (b) for the upwind RTT and the downwind RTT configuration and the fully flexible FF configurations, as well as the difference in damping to the damping to the upwind RTT configuration in the backward whirl mode (c) and the ~~foreward~~ forward whirl mode (d). The damping, as well as the damping difference, are normalized with the damping of the upwind RTT configuration at 9 ms^{-1} of the ~~foreward~~ forward whirl mode.

component of the mode shape than the backward whirl mode. When the tower flexibility is removed from the model or when the aerodynamic forces are not present, the damping of both ~~foreward~~ forward and backward modes are identical ~~.~~ (not shown

245   in Fig. 4). This indicates that the difference in ~~damping~~ whirl damping between the upwind and the downwind configuration is driven by the interaction of the aerodynamic forces on the rotor with the tower torsional motion. Other degrees of freedom such as tower bending flexibility do influence the absolute damping of the whirl modes but do not cause the major differences between the upwind and the downwind configuration.

3.3   Modal displacement effects on edgewise damping

250   The observed difference in normalized edgewise damping between the upwind and the downwind configuration presented in Fig. 4 ~~can not~~ cannot be explained with the analytical airfoil in-plane damping coefficient derived by Hansen (2007). There is no difference in the coefficient ~~, since the steady state~~ since the steady-state values of the airfoil coefficients and the ~~according~~ respective slopes are the same. Further, no difference in the in-plane velocities could be found. Thus, the difference in edgewise damping has to be explained by the out-of-plane displacements in the modes for the different turbine configurations. The out-
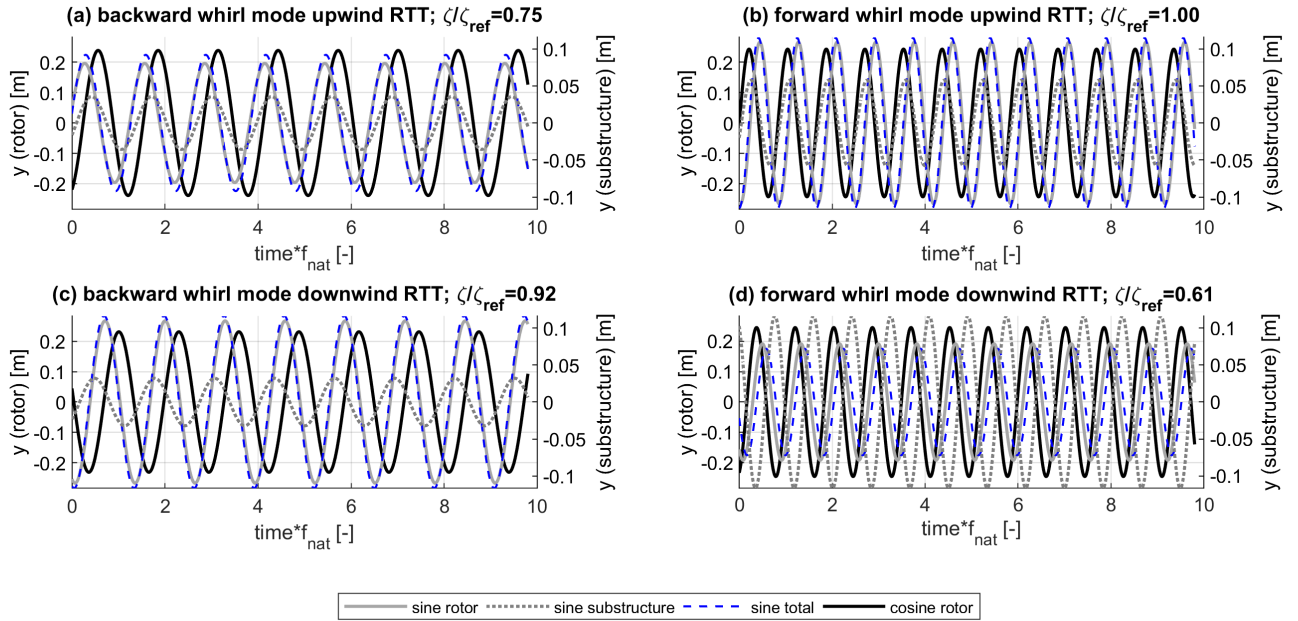
11

Figure 5. Modal out-of-plane displacements at $9 \mathrm{ms}^{-1}$ for the backward whirl mode ((a), (c)) and ~~foreward~~ forward whirl mode ((b), (d)) of the upwind RTT ((a), (b)) and downwind RTT configuration ((c), (d)). The time axis is normalized with the blade edgewise natural frequency.

255   of-plane components of the RTT configuration can be either due to the flap component in the edgewise modes ~~,~~ or due to the tower torsion that rotates the blades out of the reference plane. This section shows

- higher out-of-plane displacement gives higher edgewise damping

- difference in forcing due to configuration gives a difference in modal phases

- difference in modal phases gives a difference in damping

260   Figure 5 shows the out-of-plane displacements of the sine and cosine components of the rotor, as well as the sine displacement component due to the substructure, e.g. the tower torsion, for the backward whirl mode (Fig. 5 (a) and (c)) and the ~~foreward~~ forward whirl mode (Fig. 5 (b) and (d)) of the upwind RTT and the downwind RTT configuration.

     The figure shows that there generally is a phase shift between the sine component of the ~~out-of plane~~ out-of-plane displacement between the substructure and the rotor. Adding the two signals leads to the total sine component of the ~~out-of plane~~

265   out-of-plane displacement with the same frequency, but a different amplitude and phase. Only in the ~~foreward~~ forward whirl mode of the downwind RTT configuration, which is also the mode with the ~~over all~~ overall lowest damping, the total out-of-plane displacement is reduced due to the tower torsional displacement (Fig. 5 (d)). Generally, the main contribution to the out-of-plane displacement is due to the rotor self-motion. The ~~foreward~~ forward whirl mode (Fig. 5 (b) and (d)) shows generally higher out-of-plane displacements of ~~to~~ the substructure than the respective backward whirl mode (Fig. 5 (a) and (c)),

12

270   as the natural frequency of the ~~foreward~~ forward whirl mode is closer to the natural frequency of the second yaw mode. The natural frequencies of the modes are the same for the upwind and the downwind configuration.

The interaction of the rotor and the tower causing a higher sine out-of-plane displacement of the rotor leading to higher damping in the ~~foreward~~ forward whirl mode of the upwind RTT configuration (5 (b)) and the backward whirl mode in the downwind RTT configuration (5 (c)) than respective modes with lower sine out-of-plane displacements. The ~~foreward~~ forward whirl mode

275   of the upwind RTT configuration (5 (b)) further shows a 5% higher out-of-plane cosine component of rotor displacement than the downwind RTT configuration in the backward whirl mode (5 (c)), which explains the remaining difference in damping between the two turbine configurations.

The higher sine component of the rotor out-of-plane displacement ~~can not~~ cannot be associated with the frequency of the second yaw mode, as this does not hold true for the backward whirl mode of the downwind configuration (Fig. 5 (c)). The

280   higher out-of-plane rotor displacement in the sine component is observed to come with a sine component of the substructure out-of-plane displacement that is lagging the respective rotor displacement (Fig. 5 (b) and (c)). If the sine component of the ~~of the~~ out-of-plane displacement of the substructure is leading the respective rotor displacement the sine component of the out-of-plane rotor displacement is lower (Fig. 5 (a) and (d)).

Also the in-plane motion of the rotor (not shown here) is subject to a sine component lagging the cosine component in the

285   backward whirl mode and a sine component leading the cosine component in the ~~foreward~~ forward whirl mode. The modal velocities cause aerodynamic forces. Inherently to the whirl modes the aerodynamic in-plane forces at the hub sum up to a non-zero total in-plane force. With the arm of the shaft length, this force causes a yaw loading. Depending on the placement of the rotor relative to the yaw center a positive in-plane cosine force at the hub causes a positive yaw loading (upwind configuration) or a negative yaw loading (downwind configuration). The response of the tower, e.g. the out-of-plane substructure

290   sine component of displacement is therefore either lagging the ~~the~~ out-of-plane sine component of the rotor displacement, as in the ~~foreward~~ forward whirl mode of the upwind RTT configuration (5 (b)) and the backward whirl mode of the downwind RTT configuration (5 (c)) or the sine component of the substructure out-of-plane displacement is leading the rotor sine out-of-plane displacement (upwind RTT configuration, backward whirl mode, Fig. 5 (a) and downwind RTT configuration, ~~foreward~~ forward whirl mode, Fig. 5 (d)).

295   ~~Form this analysis~~From this analysis, it can be seen that the difference in edgewise whirl damping is due to a difference in total out-of-plane motion. The main contributor is the higher rotor out-of-plane motion associated with a favorable phasing between the out-of-plane motion of the substructure and the out-of-plane sine component of the rotor motion. It will~~therefore~~, therefore, be expected from the analysis described in the previous paragraphs, that the edgewise whirl damping can be increased by an increase of the yaw loading ~~,~~if the substructure displacement is lagging the sine out-of-plane displacement of the

300   rotor. The edgewise whirl damping is on the other hand expected to decrease with an increased yaw loading if the substructure displacement is leading the sine out-of-plane displacement of the rotor. Increasing the shaft length is expected to increase the damping of the edgewise ~~foreward~~ forward whirl mode in the upwind configuration as well as in the backward whirl mode of the downwind configuration. In the backward whirl mode of the upwind configuration and the ~~foreward~~ forward whirl mode of the downwind configuration, an increase in shaft length is expected to decrease the edgewise damping.

3.4 Parameter variation: shaft length

Figure 6 shows the normalized edgewise whirl damping values of the backward whirl mode (Fig. 6 (a) and (c)) and ~~foreward~~ forward whirl mode (Fig. 6 (b) and (d)) for the upwind RTT configuration (Fig. 6 (a) and (b)) and the downwind RTT configuration (Fig. 6 (c) and (d)) as a function of wind speed and shaft length factor. The figure shows that the normalized edgewise
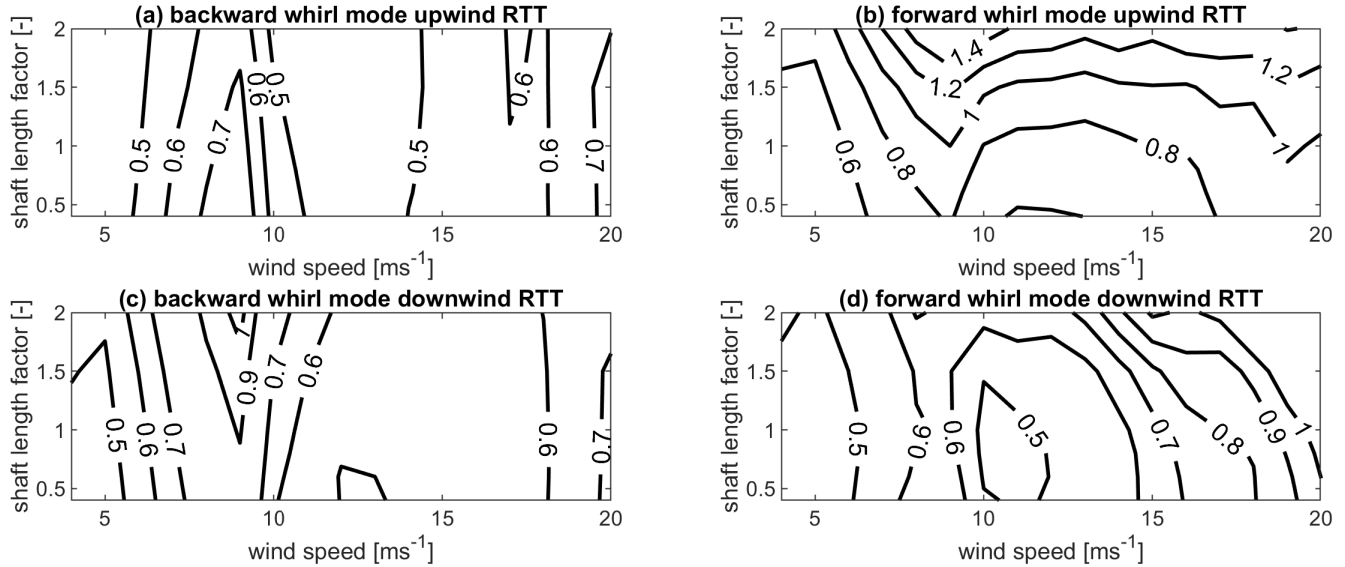

Figure 6. Normalized edgewise whirl damping ratio as a function of wind speeds and shaft length factor for the backward whirl mode ((a) and (c)) and the ~~foreward~~ forward whirl mode ((b) and (d)), for the upwind RTT configuration ((a) and (b)) and the downwind RTT configuration ((c) and (d)). The edgewise whirl damping is normalized with the damping value of ~~foreward~~ forward whirl mode in the upwind RTT configuration at a shaft length factor of 1 at $9ms^{-1}$.

whirl damping of the backward whirling mode in the upwind RTT configuration decreases with the increasing shaft length
(Fig. 6 (a)). In the downwind RTT configuration, on the other hand, the normalized edgewise whirl damping increases with the
increasing shaft length in the backward whirl mode (Fig. 6 (c)). The effect is strongest pronounced around rated wind speed.
In the forward whirl mode of the upwind RTT configuration, the normalized edgewise damping increases with the increasing
shaft length (Fig. 6 (b)). The normalized edgewise whirl damping of the downwind RTT configuration on the other hand hardly
changes with the increasing shaft length for wind speeds close to rated wind speed (Fig. 6 (d)).

For a shaft length factor of 2 and at $9ms^{-1}$ the out-of-plane displacements (see appendix Fig. A1) have been compared to the
displacements for a shaft length factor of 1 at $9ms^{-1}$ (Fig. 5). Both turbine configurations in the backward whirl mode and also
the upwind RTT configuration in the ~~foreward~~ forward whirl mode show the expected ~~dependency~~ dependence on the shaft
length according to Sect. 3.3 around rated wind speed: the normalized edgewise whirl damping of the backward whirl mode
of the downwind RTT configuration and the normalized edgewise whirl damping of the ~~foreward~~ forward whirl mode in the

320　upwind RTT configuration are increasing due to higher out-of-plane displacements in the rotor sine components. In the backward whirl mode of the upwind RTT configuration, a decrease of the sine component of the out-of-plane rotor displacements can be observed. Also for the downwind RTT configuration in the ~~foreward whirl mode~~forward whirl mode, the expected decrease of out-of-plane sine component of rotor displacement can be observed. However, an increase of the cosine out-of-plane displacements of the rotor can also be seen. The combination of the out-of-plane displacements leads to the effect that hardly

325　any difference in edgewise whirl damping can be observed at around rated wind speed for the ~~foreward~~ forward whirl mode of the downwind RTT configuration.

3.5　Parameter variation: cone angle

Figure 7 shows the normalized edgewise whirl damping for the backward whirl mode (Fig. 7 (a) and (c)) and the forward whirl mode (Fig. 7 (b) and (d)) in the upwind RTT (Fig. 7 (a) and (b)) and the downwind RTT configuration (Fig. 7 (c) and (d)) as a function of cone angle and wind speed.
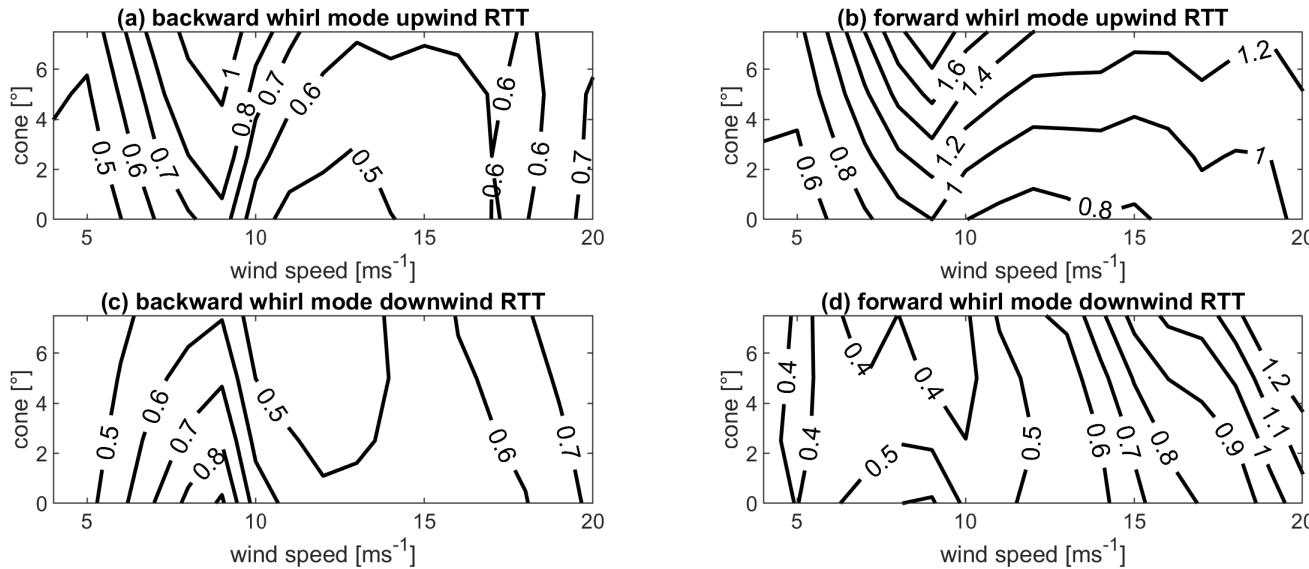

Figure 7. Normalized edgewise whirl damping as a function wind speeds and cone angle for the backward whirl mode ((a) and (c)) and the ~~foreward~~ forward whirl mode ((b) and (d)), for the upwind RTT configuration ((a) and (b)) and the downwind RTT configuration ((c) and (d)). The whirl damping is normalized with the damping value of ~~foreward~~ forward whirl mode in the upwind configuration at $0°$ at $9\ ms^{-1}$.

330

　　The figure shows that the edgewise whirl damping of both modes increases with an increasing cone angle in the upwind RTT configuration (Fig. 7 (a) and (b)). In the downwind RTT configuration the edgewise whirl damping decreases with increasing cone angle for wind speeds around rated wind speed (Fig. 7 (c) and (d)).

Introducing the cone angle has several effects. On the one hand, the cone angle changes the ~~steady state~~ steady-state values of

335   the airfoil coefficients and therefore the estimated analytical damping coefficient by Hansen (2007): The blades deflect against the coning direction in the upwind RTT configuration, while the blades deflect in the same direction as the cone direction in the downwind RTT configuration. The analytical damping coefficient of the r/R=75% airfoil at 9ms^{-1} has decreased by 33% in the upwind RTT configuration when a cone angle of 7.5° is introduced. The analytical damping coefficient of the r/R=75% airfoil at 9ms^{-1} has increased by 38% in the downwind RTT configuration when a cone angle of 7.5° is introduced. On the other

340   hand, the cone angle also changes the coupling between the in-plane loading and the tower torsion as the distance between the yaw axis and the outboard airfoils is increased. Comparing the displacements at 9ms^{-1} at a cone angle of 7.5° (Fig. A2) with the out-of-plane displacements at 9ms^{-1} without cone angle (Fig. 5) shows only very little changes in the rotor sine components of the out-of-plane displacements. However, the downwind RTT configuration shows a significant decrease in the cosine component of the out-of-plane rotor displacements, while the upwind RTT configuration shows a significant increase in

345   the cosine out-of-plane rotor displacements when the cone angle of 7.5° is introduced. The changes in the cosine out-of-plane rotor displacement dominate the change in normalized edgewise whirl damping.

3.6   Parameter variation: tower torsion

Figure 8 shows the normalized edgewise whirl damping for the backward whirl mode (Fig. 8 (a) and (d)) and ~~foreward~~ forward whirl mode (Fig. 8 (b) and (c)) of the upwind RTT (Fig. 8 (a) and (b)) and downwind RTT configuration (Fig. 8 (c) and (d)) as

350   a function wind speed and tower torsion stiffness factor.

    While the normalized edgewise whirl damping is increasing in the backward whirl mode of the upwind RTT configuration with the increasing tower torsional stiffness (Fig. 8 (a)), the normalized edgewise damping of the backward whirl mode of the downwind RTT configuration (Fig. 8 (c)) is decreasing with increasing tower torsional stiffness at around rated wind speed. For high wind speeds and ~~a~~ stiffness factors lower than 0.5 the edgewise damping of the backward whirl mode increases drastically

355   with the decreasing tower torsional stiffness for both configurations. In the ~~foreward whirl mode~~ forward whirl mode, the normalized edgewise damping generally decreases in both configurations with an increasing tower torsional stiffness (Fig. 8 (b) and (d)). Both configurations in the ~~foreward~~ forward whirl mode show an area at around cut-out wind speeds at a stiffness factor at around 0.5, where a local maximum of normalized edgewise damping is reached.

    Comparing Fig. A3 with Fig.5 shows that a decrease of tower torsional stiffness to a factor of 0.2 at 9 ms^{-1} increases generally

360   the out-of-plane displacements associated with the substructure. Further, phasing between the substructure and rotor out-of-plane displacement as well as the rotor associated out-of-plane displacement is changing. ~~Over all~~Overall, only the upwind RTT configuration in the backward whirl mode does not benefit from the decrease in the tower torsional stiffness in the out-of-plane displacements at 9 ms^{-1}. At high wind speeds, the effect of the frequency placement can be observed. As the tower torsional stiffness decreases below a factor of around 0.5 the second yaw frequency crosses the edgewise ~~foreward~~ forward

365   whirl mode frequency and moves closer to the edgewise backward whirl mode frequency. Thus, the highest damping at high wind speeds is observed at ~~at~~ a stiffness factor of around 0.5 for high wind speeds.
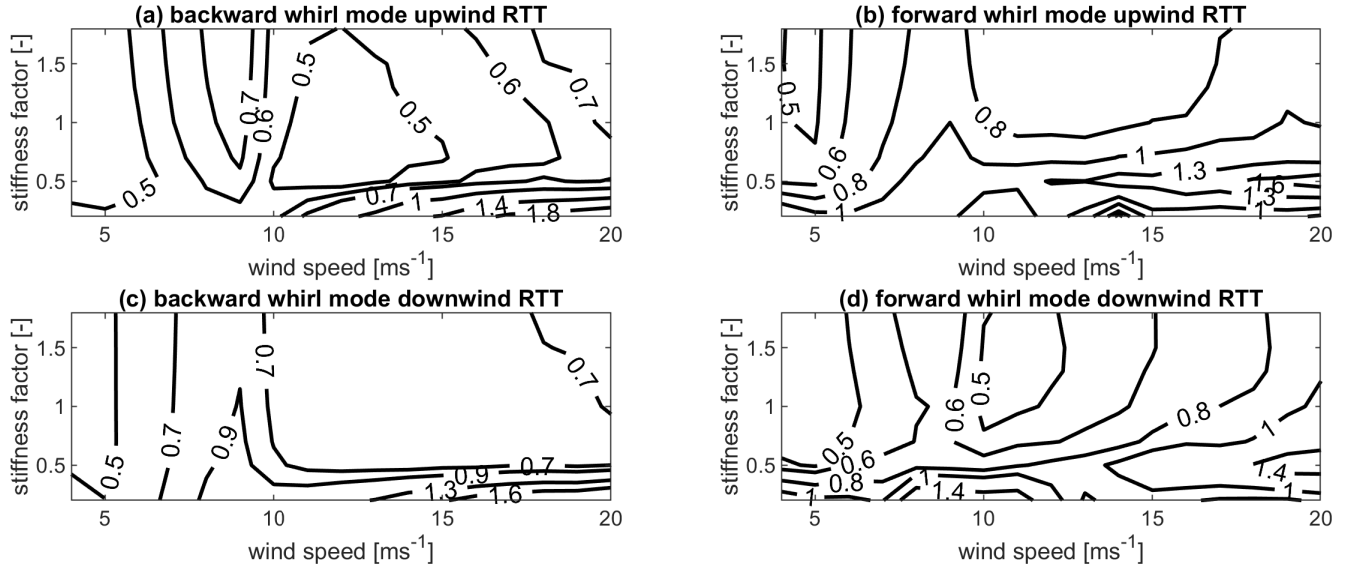
Figure 8. Normalized edgewise whirl damping as a function of wind speeds and tower torsion stiffness factor for the backward whirl mode ((a) and (c)) and the ~~foreward~~ forward whirl mode ((b) and (d)), for the upwind RTT configuration ((a) and (b)) and the downwind RTT configuration ((c) and (d)). The whirl damping is normalized with the damping value of ~~foreward~~ forward whirl mode in the upwind RTT configuration at a tower torsion stiffness factor of 1 at 9 ms^{-1}.

4 Summary

In this article, the change in edgewise whirl damping when an upwind wind turbine is converted into a downwind configuration has been investigated on the example of a simplified version of the commercial Suzlon S111 2.1MW wind turbine. The edge-
370 wise forward whirl mode has been shown to decrease in damping as the upwind configuration is changed into the downwind configuration. The edgewise backward whirl mode, on the other hand, has been seen to increase in damping when the upwind configuration is changed into a downwind configuration. The interaction with the aerodynamic forces, the rotor and tower torsional motion have been shown to create a difference in out-of-plane displacement. The out-of-plane displacement was seen to cause the observed differences in edgewise damping.

375 The difference in the ~~out-of plane~~ out-of-plane displacements and therefore damping was shown to increase with an increased shaft length, as the yaw loading from the in-plane cosine shear forces could be increased. An increase in cone angle has been shown to increase the cosine component of the out-of-plane rotor displacements and therefore damping for the upwind configuration, while the increase in cone causes a decrease in cosine component of the out-of-plane displacements and damping in the downwind configuration. A decrease in tower torsional stiffness has been seen to increase the damping from a ~~favourable~~
380 favorable placement of natural frequencies relative to each other, as long as the rotor and substructure out-of-plane displacement do not counteract each other due to phase differences.

5 Conclusion and future work

As a decrease in damping increases extreme as well as fatigue loads, the edgewise damping should be included in the design considerations. For the shaft length, there would be a trade-off between edgewise damping of the two modes, but also the
385 rotor overhanging moment that has to be carried by the support structure. The consideration of edgewise damping would suggest a higher cone angle for upwind configurations than for downwind configurations. Again, other considerations like tower clearance, flapwise blade root loads and power production compete in the design decision. From an edgewise damping point of view downwind configurations could benefit from towers with lower torsional stiffness. Replacing a tubular tower or the bottom segments of the tubular tower by a lattice structure could significantly increase the overall edgewise damping. However,
390 a full load assessment is required to also investigate the influence on other load sensors than the edgewise blade loads.
~~The~~ It should be pointed out, that the damping of the ~~first two~~ edgewise whirl modes ~~has been estimated from timeseries where the foreward or backward whirl mode are excited. Using the same model as used for load simulations has the advantage of estimating directly the differences in damping without linearization effects. However, this method will only~~ and especially the mode shapes are turbine specific. However, it can generally be concluded that upwind and downwind configurations are
395 expected to have different out-of-plane displacements due to the structural arrangement of the tower center relative to the rotor center. The tower torsion will have a great impact on the difference in edgewise whirl damping between the upwind and the downwind configuration. Tower torsional stiffness, cone angle and shaft length will be able to ~~estimate the damping, if clearly only one mode is excited and only one frequency dominates the spectrum. Further the damping has to be so low, that the peak to peak counting and amplitude detection can be reliably performed.In this study normalized edgewise damping~~
400 ~~above a normalized damping of 1.8 could not be estimated . This limited effectively the investigated range of the investigated parameter. The edgewise modes are~~ influence the difference in edgewise whirl damping. How large the impact is of each parameter individually or relative to each other is depends heavily on the individual turbines mode shapes and frequency placement.

The damping of the first two edgewise whirl modes has been estimated from time-series where the forward or backward whirl
405 mode i excited. The chosen example turbine was well suited for ~~this method as they~~ the investigations since the edgewise whirl modes are significantly lower damped than other modes and no other frequency was placed close by the edgewise whirl frequencies. Estimating the damping from an eigenvalue solution would eliminate these limitations and broader investigations also regarding other turbines classes and rated power could be made.
~~Future work should investigate further the reason for the different out-of-plane displacement in the mode shapes, especially the~~
410 ~~differences observed in the cosine components of the out-of-plane displacement. Further the~~ Further, the degrees of freedom of the turbine model should be extended to the full flexibility, as additional degrees of freedom are expected to affect the mode shapes, especially the turbine tilting flexibility (tower fore-aft and shaft bending flexibility), or shaft bending ~~and~~ are expected to influence the out-of-plane displacements. The tower side-side deflection can be expected to couple directly to the asymmetric edgewise motion. The tower side-side deflection could further be expected to couple to out-of-plane displacement through the
415 yaw motion, as the center of gravity of the rotor is not at the tower center. Also, the shaft torsional flexibility could influence

the edgewise damping. Further investigations should evaluate the influence of the upper especially on the mode shapes of the whirl modes.

Future work should investigate further the reason for the different out-of-plane displacement in the mode shapes, especially the differences observed in the cosine components of the out-of-plane displacement. Gaining a full understanding of the

420 out-of-plane displacement is important as it enables to design wind turbines with higher damping and therefore lower fatigue and extreme loads.

Appendix: Out-of-plane displacements for parameter variations

425 The following figures show the out-of-plane displacements of the two edgewise damping modes in the two RTT configurations at $9\mathrm{ms}^{-1}$ for a shaft length factor of 2 (Fig. A1), a cone angle of $7.5°$ (Fig. A2) and a tower torsional stiffness factor of 0.2 (Fig. A3).

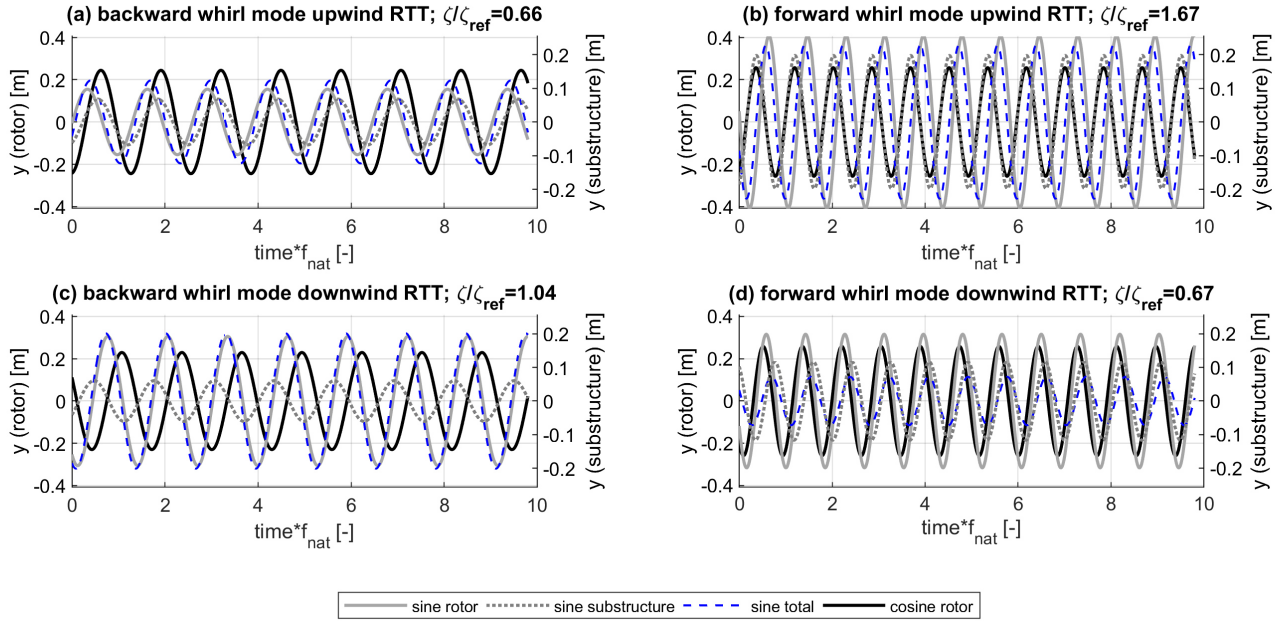**Figure A1.** Modal out-of-plane displacements at 9ms^{-1} and a shaft length factor of 2 for the backward whirl mode and ~~foreward~~ forward whirl mode of the upwind RTT and downwind RTT configuration. The time axis is normalized with the blade edgewise natural frequency.
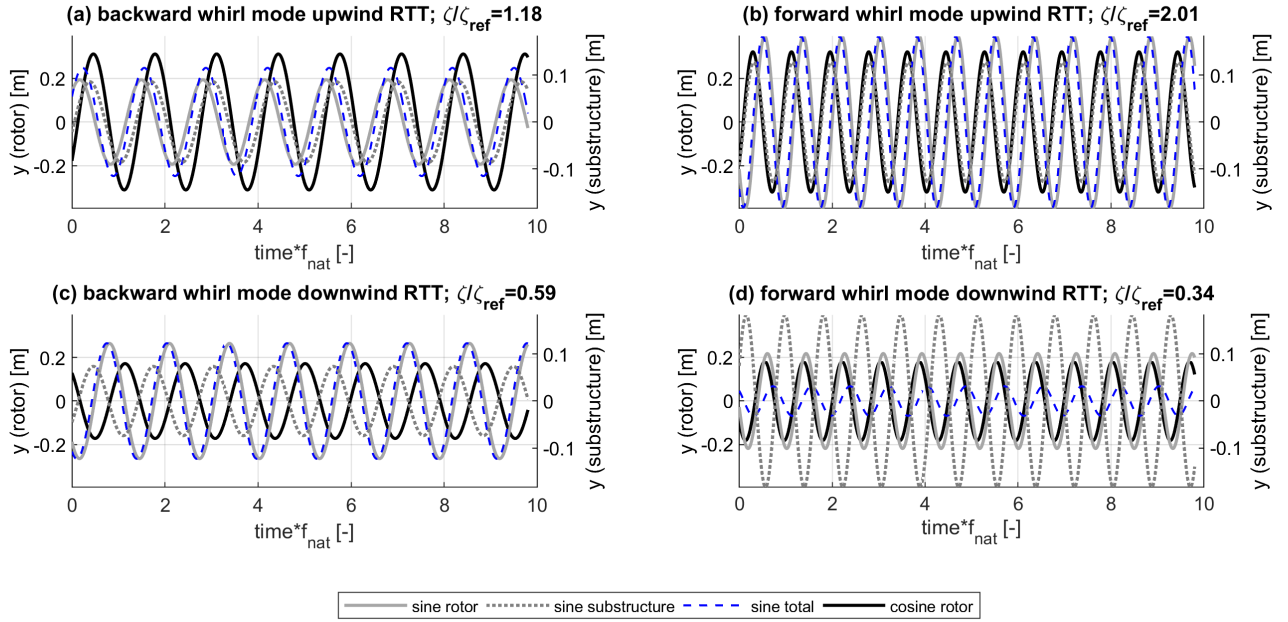
Figure A2. Modal out-of-plane displacements at $9\,\text{ms}^{-1}$ and a cone angle of $7.5°$ for the backward whirl mode and ~~foreward~~ forward whirl mode of the upwind RTT and downwind RTT configuration. The time axis is normalized with the blade edgewise natural frequency.
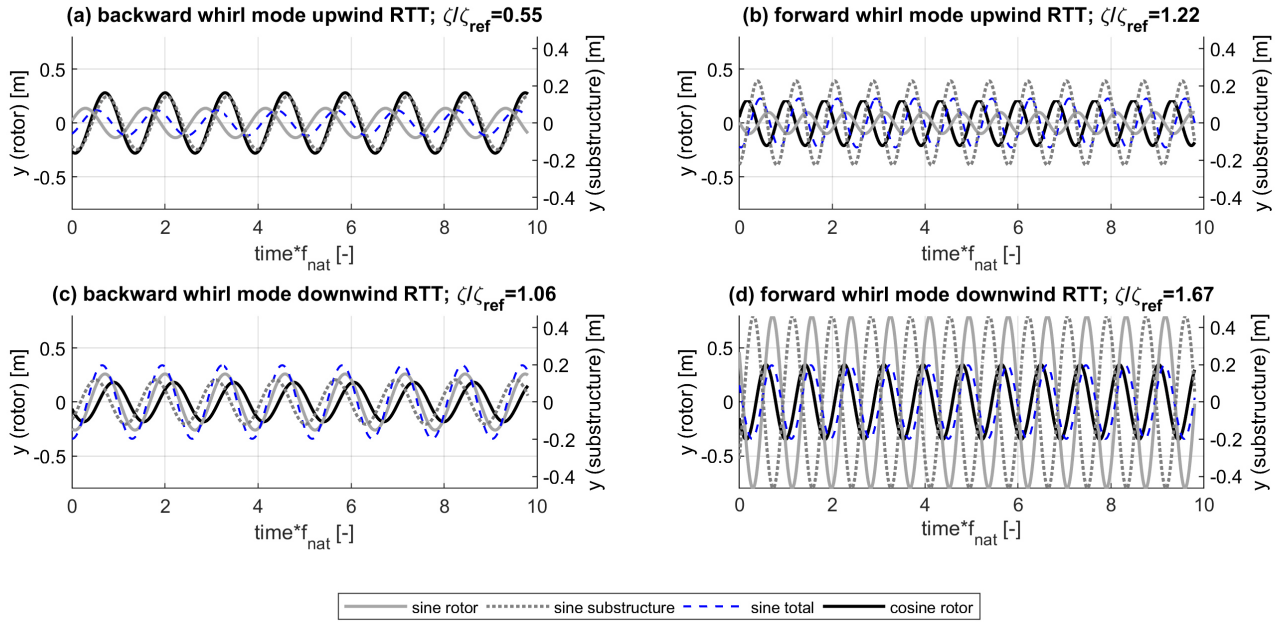
Figure A3. Modal out-of-plane displacements at 9ms^{-1} and a tower torsional stiffness factor of 0.2 for the backward whirl mode and ~~foreward~~ forward whirl mode of the upwind RTT and downwind RTT configuration. The time axis is normalized with the blade edgewise natural frequency.

Author contributions. GW set-up the models and carried out the calculations. LB and DV revised the models. All authors have interpreted the obtained data. GW prepared the paper with revisions of all co-authors.

References

Bir, G.: Multiblade Coordinate Transformation and Its Application to Wind Turbine Analysis, Report NREL/CP-500-42553, 2008.

Glasgow, J., Miller, D., and Corrigan, R.: Comparison of upwind and downwind rotor operations of the DOE/NASA l00-kW MOD-0 wind
435   turbine, NASA Report; No. TM-8744; p. 225–234, 1981.

Hansen, M. H.: Improved Modal Dynamics of Wind Turbines to Avoid Stall-induced Vibrations, Wind Energy; Vol. 6; p. 179-195,
    https://doi.org/10.1002/we.79, 2003.

Hansen, M. H.: Aeroelastic Stability Analysis of Wind Turbines Using an Eigenvalue Approach, Wind Energy; Vol. 7; p. 133-143,
    https://doi.org/10.1002/we116, 2004.

440   Hansen, M. H.: Aeroelastic instability problems for wind turbines, Wind Energy; Vol. 10; Nr. 6; p. 551-577, https://doi.org/10.1002/we.242,
    2007.

Madsen, H. A., Larsen, T. J., Pirrung, G. R., Li, A., and Zahle, F.: Implementation of the Blade Element Momentum Model on a Polar Grid
    and its Aeroelastic Load Impact, Wind Energy Science; Vol. 5; p.1-27, https://doi.org/10.5194/wes-5-1-2020, 2020.

MathWorks: fft, Matlab Documentation, https://se.mathworks.com/help/matlab/ref/fft.html, 2020.

445   Petersen, J. T., Madsen, H. A., Bjoerck, H. A., Enevoldsen, P., Øye, S., Ganander, H., and Winkelaar, D.: Prediction of dynamic loads and
    induced vibrations in stall, Risø-Report (Risø-R-1045(EN)), 1998a.

Petersen, J. T., Thomsen, K., and Madsen, H. A.: Local blade whirl and global rotor whirl interaction, Risø-Report (Risø-R-1067(EN)),
    1998b.

Reiso, M. and Muskulus, M.: The simultaneous effect of a fairing tower and increased blade flexibility on a downwind mounted rotor, Journal
450   of Renewable and Sustainable Energy; Vol. 5; p. 033106-1–1033106-11, https://doi.org/10.1063/1.4803749, 2013.

Thomsen, K., Petersen, J. T., Nim, E., Øye, S., and Petersen, B.: A Method for Determination of Damping for Edgewise Blade Vibrations,
    Wind Energy, https://doi.org/10.1002/we.42, 2000.

Wanke, G., Bergami, L., Larsen, T. J., and Hansen, M.: Changes in design driving load cases: Operating an upwind turbine with a downwind
    rotor configuration, Wind Energy, https://doi.org/10.1002/we.2384, 2019.

455   Zahle, F., Madsen, H., and Sørensen, N.: Evaluation of tower shadow effects on various wind turbine concepts, Research in Aeroelasticity
    DTU Report EFP-2007-II; Vol. 1698; p.1–147, 2009.

Configurations and parameter variations configuration/ parameter variation propertiesedgewise damping estimation all configurations no tilt, no cone, no prebendsimplified controller, no gravity, uniform inflow(no turbulence, no sheer, no veer, no inclination angle)upwind FF upwind, all degrees of freedom (fully flexible)downwind FF downwind, all degrees of freedom (fully
460   flexible) upwind RTT upwind, rotor flexibility, tower torsion flexibilitydownwind RTT downwind, rotor flexibility, tower torsion flexibilityparameter variation shaft length up- and downwind RTT configurationshaft length variation: -30% to +100% cone angle up- and downwind RTT configurationcone angle variation: 0° to 7.5° (away from tower)tower torsional stiffness up- and downwind RTT configurationtorsional stiffness factor variation ± 80%